

Article

A Novel Advancing Signal Processing Method Based on Coupled Multi-Stable Stochastic Resonance for Fault Detection

Hongjiang Cui ¹, Ying Guan ¹, Huayue Chen ^{2,*} and Wu Deng ^{3,*} 

¹ School of Locomotive and Rolling Stock Engineering, Dalian Jiaotong University, Dalian 116028, China; chj@djtu.edu.cn (H.C.); guanying2017@djtu.edu.cn (Y.G.)

² School of Computer Science, China West Normal University, Nanchong 637002, China

³ School of Electronic Information and Automation, Civil Aviation University of China, Tianjin 300300, China

* Correspondence: sunnyxiaoyue20@cwnu.edu.cn (H.C.); dw7689@163.com (W.D.)

Abstract: In recent years, methods for detecting motor bearing faults have attracted increasing attention. However, it is very difficult to detect the faults from weak motor bearing signals under the strong noise. Stochastic resonance (SR) is a popular signal processing method, which can process weak signals with the noise, but the traditional SR is burdensome in determining its parameters. Therefore, in this paper, a new advancing coupled multi-stable stochastic resonance method, with two first-order multi-stable stochastic resonance systems, namely CMSR, is proposed to detect motor bearing faults. Firstly, the effects of the output signal-to-noise ratio (SNR) for system parameters and coupling coefficients are analyzed in-depth by numerical simulation technology. Then, the SNR is considered as the fitness function for the seeker optimization algorithm (SOA), which can adaptively optimize and determine the system parameters of the SR by using the subsampling technique. An advancing coupled multi-stable stochastic resonance method is realized, and the pre-processed signal is input into the CMSR to detect the faults of motor bearings by using Fourier transform. The faults of motor bearings are determined according to the output signal. Finally, the actual vibration data of induction motor bearings are used to prove the effectiveness of the proposed CMSR. The comparison results with the MSR show that the CMSR can obtain a higher output SNR, which is more beneficial to extract weak signal features and realize fault detection. At the same time, this method also has practical application value for engineering rotating machinery.

Keywords: motor bearings; signal processing; fault detection; stochastic resonance; signal-to-noise ratio; seeker optimization



Citation: Cui, H.; Guan, Y.; Chen, H.; Deng, W. A Novel Advancing Signal Processing Method Based on Coupled Multi-Stable Stochastic Resonance for Fault Detection. *Appl. Sci.* **2021**, *11*, 5385. <https://doi.org/10.3390/app11125385>

Academic Editor: Andrzej Bień

Received: 30 May 2021

Accepted: 7 June 2021

Published: 10 June 2021

Publisher's Note: MDPI stays neutral with regard to jurisdictional claims in published maps and institutional affiliations.



Copyright: © 2021 by the authors. Licensee MDPI, Basel, Switzerland. This article is an open access article distributed under the terms and conditions of the Creative Commons Attribution (CC BY) license (<https://creativecommons.org/licenses/by/4.0/>).

1. Introduction

Due to the harsh working environment, the rolling bearings, which are a core part of rotating machinery, often suffer different damages, which have serious consequences for safety and the economy [1–3]. Therefore, it is indispensable for monitoring the bearing and extracting weak signals from it.

Extracting useful signal features under the strong noise background is called weak signal detection [4–7]. The traditional signal processing methods usually start with noise reduction, such as empirical mode decomposition, wavelet transform, spectral kurtosis, singular value decomposition, variational mode decomposition, and some signal analysis methods with optimization algorithms [8–13], which unavoidably weakens the feature information of useful signals. Unlike the traditional procedures for weak characteristic signals covered by noise, stochastic resonance (SR) [14] can make signals obviously by bypassing the noise. It is widely used in weak signal detection, especially in the field of fault diagnosis. However, subject to the adiabatic approximation, the input signal frequency of SR must be much less than 1 Hz [15]. To detect large frequency signals using SR theory, the re-scaling frequency SR (RFSR) method is proposed in [16], where the original sampling and characteristic frequencies are separated using R parameters. Li et al. [17] introduced

an adaptive step-changed SR (SCSR), in which they use the entropy index to quantify SR performance. Tan et al. [18] explained frequency-shifted and re-scaling SR. Wang et al. [19] analyzed the multi-scale noise-regulated SR. For the detection of multi-frequency signals, Shi et al. [20] used SR tuning multi-scale noise. The above methods use SR to play an important role in practical engineering applications. Other signal analysis methods are also proposed to process signals [21–26].

In the process of using SR to detect weak signals, new parameter optimization methods and SR models have been continuously proposed. Li et al. [27] presented overdamped multi-stable stochastic resonance (MSR) with a tri-stable potential. Han et al. [28] introduced an MSR system which is applied to multi-frequency weak signal detection. In addition, some scholars have also studied the second-order SR system. Lu et al. [29] analyzed the detection of weak signals in a second-order underdamped variable-step SR system. Lei et al. [30] further studied the second-order MSR method and used it for the early fault diagnosis of bearings. Except for the first-order and second-order SR models, scholars have studied coupled SR systems less. The coupled SR system is an analysis of the SR model from another scale. Zhang et al. [31] applied the coupling bi-stable system for weak signal extraction, and the result shows that the coupled bi-stable SR is better in terms of detection effect than a single bi-stable SR system. Li et al. [32] further studied an adaptive coupling bi-stable SR method and its application. Zhang [33] analyzed a coupled bi-stable SR system under Lévy noise. In addition, some combination methods with other algorithms have been proposed in recent years [34–38].

In sum, the SR, MSR, SNR, coupled SR system, et cetera, are proposed by some researchers to best detect motor bearing faults. These methods can better detect motor bearing faults, but they find it very difficult to detect the faults from weak motor bearing signals under the strong noise. For solving this problem, in this paper, a new advancing coupled multi-stable stochastic resonance method, with two first-order multi-stable stochastic resonance systems, namely the CMSR, is proposed to detect motor bearing faults. In this proposed CMSR, the effects of the output signal-to-noise ratio (SNR) for system parameters and coupling coefficients, are analyzed in-depth by numerical simulation technology. Then, the SOA is used to adaptively optimize and determine the system parameters of the SR by using the subsampling technique. Finally, the pre-processed signal is input into the CMSR to detect the faults of motor bearings by Fourier transform.

The innovations and main contributions of this paper are described as follows:

- A novel advancing signal processing method based on coupled multi-stable stochastic resonance is proposed to detect the faults of motor bearings;
- The output signal-to-noise ratio (SNR) for system parameters and coupling coefficients are analyzed in depth;
- The SOA is used to adaptively optimize and determine the system parameters of the SR by using the subsampling technique;
- The actual vibration data of induction motor bearings are used to prove the effectiveness of the proposed CMSR system.

The rest of the paper is organized as follows. The first-order MSR system, the CMSR system, and the relationship between them, are briefly introduced in Section 2 in order to understand the CMSR system more intuitively. In Section 3, the measurement index of the SR system, the influence of system parameters on the CMSR system, and the application of the seeker optimization algorithm (SOA) in the SR systems are analyzed. In Section 4, the bearing inner race and rolling element fault data are processed by the CMSR system and compared with the MSR system in order to prove the effectiveness of the CMSR. Finally, Section 5 summarizes the conclusion.

2. Theoretical Background

2.1. First-Order MSR System Model

The MSR model has periodicity and multiple potential barriers and potential wells. It can effectively avoid output saturation by independently adjusting system parameters. The first-order MSR system model is expressed as follows [39–41]

$$\frac{dx}{dt} = -U'(x) + s(t) + n(t) \tag{1}$$

where $s(t)$ is the input signal, $n(t)$ represents the Gaussian white noise, $x(t)$ is the final output, and $U(x)$ is the periodic potential function. The specific expression of $U(x)$ is given as follows

$$U(x) = -a \cos(bx) \tag{2}$$

where a and b are positive real numbers. Let $a = b = 1$; $U(x)$ is shown in Figure 1. The periodic potential function has several potential barriers and potential wells can be found from it.

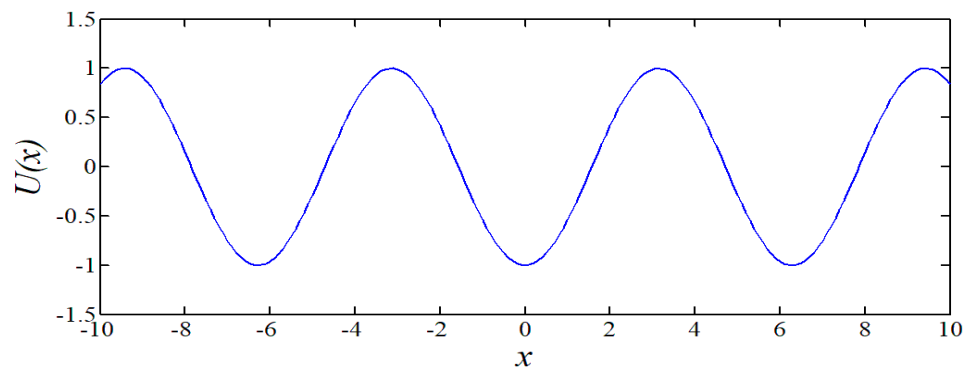


Figure 1. Periodic potential function.

The following Formula (3) can replace the Equation (1)

$$\frac{dx}{dt} = -ab \sin(bx) + s(t) + n(t) \tag{3}$$

The Runge–Kutta method is used in Equation (3), and the specific calculation process is given as follows:

$$\begin{cases} k_1 = h(-ab \sin(bx_n) + s_n + n_n) \\ k_2 = h(-ab \sin(b(x_n + \frac{1}{2}k_1)) + s_n + n_n) \\ k_3 = h(-ab \sin(b(x_n + \frac{1}{2}k_2)) + s_{n+1} + n_{n+1}) \\ k_4 = h(-ab \sin(b(x_n + k_3)) + s_{n+1} + n_{n+1}) \\ x_{n+1} = x_n + \frac{1}{6}(k_1 + 2k_2 + 2k_3 + k_4) \end{cases} \tag{4}$$

In Formula (4) s_n and n_n represent the input signal and noise, respectively. x_n is the output signal and h is the iterative step of the numerical calculation.

2.2. Mode of CMSR System

The CMSR system consists of two first-order MSR systems whose specific expressions are described as follows [42,43]

$$\begin{cases} \frac{dx}{dt} = -a_0b_0 \sin(b_0x) + r(y - x) + s(t) + n(t) \\ \frac{dy}{dt} = -ab \sin(by) + r(y - x) \end{cases} \tag{5}$$

where the $-a_0b_0 \sin(b_0x)$ is the controlled system, the parameters a_0 and b_0 are fixed values, which are set $a_0 = b_0 = 1$. The system where the $-ab \sin(by)$ is located is the control system and $r(y - x)$ indicates that the y -channel input signal is used to adjust the x -channel input signal. The parameter variables are a and b , and the final output of the CMSR system is x due to the signal and noise acting on the controlled system. Among them there is given, as follows:

$$\begin{cases} U_1(x) = -a_0 \cos(b_0x) \\ U_2(y) = -a \cos(by) \end{cases} \tag{6}$$

When the signal noise and system parameters match each other to produce a SR phenomenon the potential function $U(x, y)$ is obtained as follows:

$$U(x, y) = -a_0 \cos(b_0x) - a \cos(by) + \frac{r}{2}(x^2 - y^2) \tag{7}$$

When there are $a_0 = b_0 = 1, a = b = 1, r = 0.1$, the potential function diagram is shown in Figure 2. It is found that the active range of the particles is increased, the noise utilization rate is increased, and the dynamic performance is more abundant when compared Figures 1 and 2.

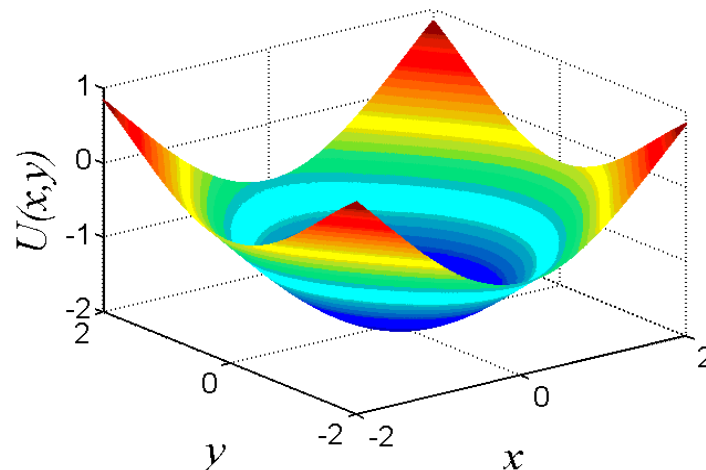


Figure 2. Potential function.

For the solution of Equation (5), the Runge–Kutta method is still used and the specific solution is obtained as follows

$$\begin{cases} k_1 = h[-\sin(x_n) + r(y_n - x_n) + s_n] \\ l_1 = h[-ab \sin(by_n) + r(y_n - x_n)] \\ k_2 = h[-\sin((x_n + 0.5k_1) + r(y_n - (x_n + 0.5k_1)) + s_n] \\ l_2 = h[-ab \sin(b(y_n + 0.5l_1)) + r((y_n + 0.5l_1) - x_n)] \\ k_3 = h[-\sin((x_n + 0.5k_2) + r(y_n - (x_n + 0.5k_2)) + s_{n+1}] \\ l_3 = h[-ab \sin(b(y_n + 0.5l_2)) + r((y_n + 0.5l_2) - x_n)] \\ k_4 = h[-\sin((x_n + k_3) + r(y_n - (x_n + k_3)) + s_{n+1}] \\ l_4 = h[-ab \sin(b(y_n + l_3)) + r((y_n + l_3) - x_n)] \\ x_{n+1} = x_n + \frac{1}{6}(k_1 + 2k_2 + 2k_3 + k_4) \\ y_{n+1} = y_n + \frac{1}{6}(l_1 + 2l_2 + 2l_3 + l_4) \end{cases} \tag{8}$$

where s_n and n_n represent the input signal and noise, respectively. x_n is the output signal and h is the iterative step of the numerical calculation.

2.3. System Measurement Index

SOA uses the output *SNR* as the system measurement index [44]. When the noise component is less, the *SNR* is larger, and the effect of the SR system is better. The *SNR* output can be explained as follows [45–47]

$$X(k) = \sum_{n=1}^N x(n) e^{-j2\pi(k-1)(n-1)/N}, 1 \leq k \leq N \quad (9)$$

where $x(n)$ is the output signal of the SR system, $X(k)$ is obtained by Fourier transform and n is the signal length.

$$Y(k) = \frac{2|X(k)|}{N}, 1 \leq k \leq \frac{N}{2} \quad (10)$$

$$K_0 = \frac{f_{\max} \times N}{f_s} + 1 \quad (11)$$

At the signal frequency f_{\max} , K_0 is the peak number of its spectrum and f_s is the sampling frequency. $Y(k)$ is the magnitude of the signal amplitude spectrum. *SNR* can be expressed as follows:

$$SNR = 10 \lg \frac{Y(K_0)}{\sum_{k=1}^{N/2} Y(k) - Y(K_0)} \quad (12)$$

2.4. The Flow of the CMSR System

The flow of the advancing coupled multi-stable stochastic resonance method with two first-order multi-stable stochastic resonance systems (CMSR) is shown in Figure 3.

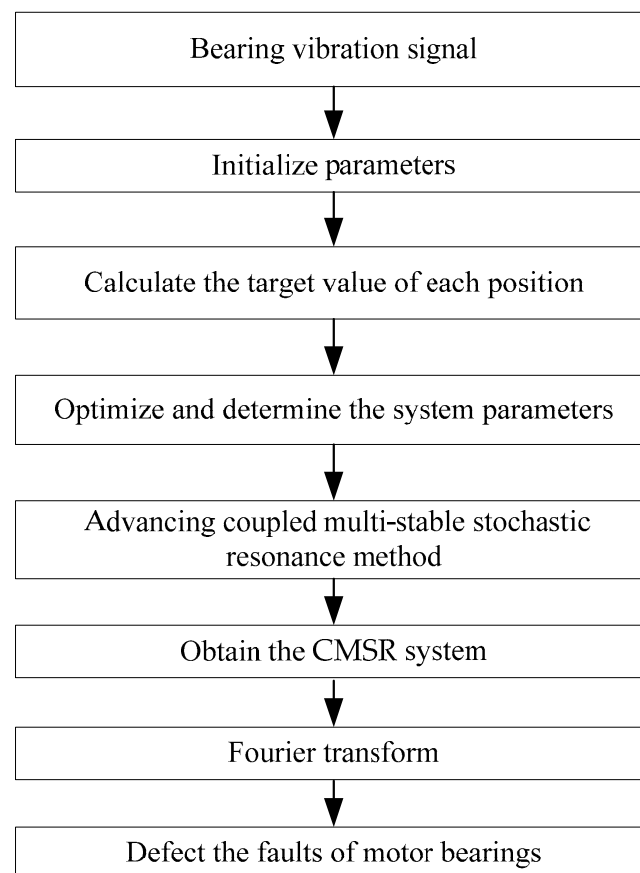


Figure 3. The flow of the CMSR system.

The flow of the CMSR system in Figure 3 shows that a , b and r can affect the performance of the CMSR system. Based on the adiabatic approximation theory of SR, the variable-scale method can be used to introduce the frequency compression ratio (R) to convert large frequency signals into small frequency signals. For the selection of parameters a , b , r , R , this paper uses the SOA, which takes output SNR as the fitness function to optimize four parameters synchronously. The SOA process includes the determination of search step-size and search direction, the update of the individual position of the seeker, and the implementation of the algorithm. The specific procedures are described as follows:

- Signal preprocessing. The envelope signal obtained after filtering and demodulating the collected bearing vibration signal is recorded as s_1 , $s_2 = s_1 - \text{mean}(s_1)$, $s = s_2 / 2\max(\text{abs}(s_2))$, S is the input signal;
- Parameter initialization. Number of iterations, population size, and range of parameters are determined;
- Calculate the target value of each position using the output SNR formula;
- Parameter optimization. The SNR is considered as the fitness function of the seeker optimization algorithm (SOA) to adaptively optimize and determine the system parameters of the SR by using the subsampling technique;
- If the set value is equal to the current number of iterations, output the best system parameters a , b , r , R and enter the next step; otherwise, return to the previous step;
- Signal detection. Import the pre-processed signal into the CMSR system with the determined parameters to get the output signal x_1 Scale recovery of signal frequency and amplitude $x = x_1 \times 2\max(\text{abs}(s_2))$;
- Fault detection. Fourier transform of x to complete fault detection.

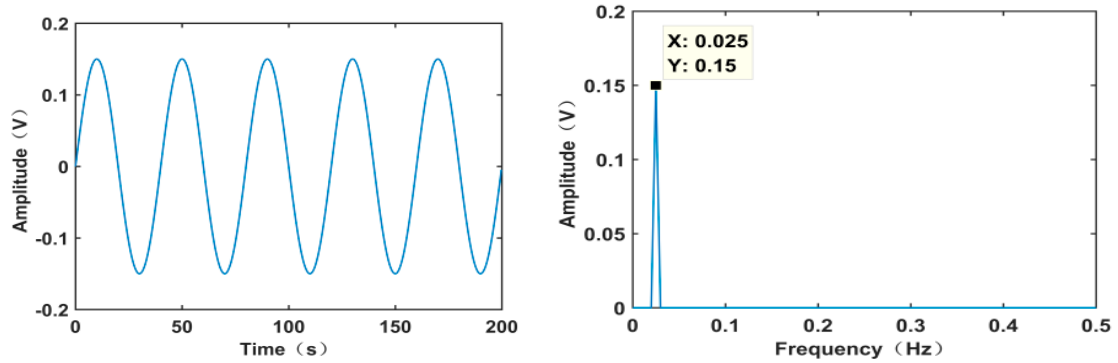
3. System Parameter Analysis

The input signal must strictly satisfy an amplitude of less than 1 and a frequency of less than 1 Hz because of the adiabatic approximation theory of SR. Therefore, it is necessary to understand the relationship between system parameters and SR output by simulating small parameter signals. Let the signal be

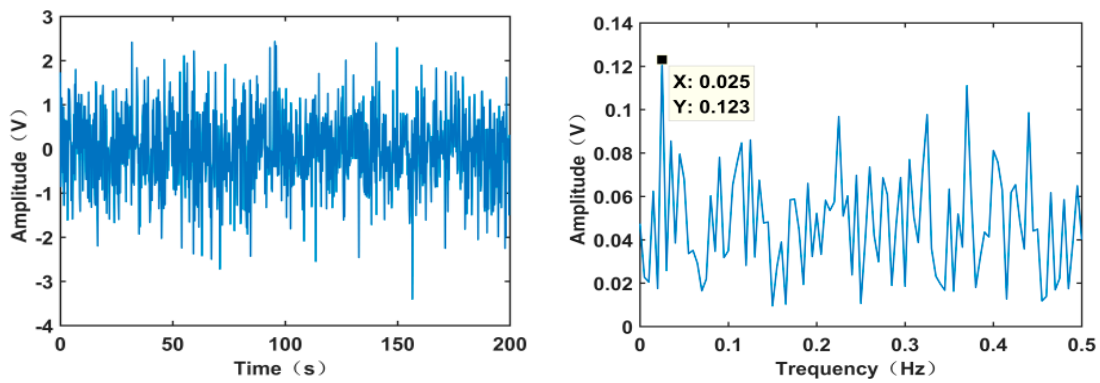
$$s(t) = A \sin(2\pi f_0 t) + n(t) \quad (13)$$

where $n(t)$ is the Gaussian white noise, the signal amplitude is $A = 0.15$, $f_0 = 0.025$, and the noise intensity is $D = 0.4$.

The time domain waveform and amplitude spectrum of noiseless signal are shown in Figure 4a, and Figure 4b displays them with the noisy signal. In Figure 4b, the periodicity of signal and $f_0 = 0.025$ Hz cannot be resolved. The SNR calculated by Equation (12) is -22.9 dB. In order to better analyze the relationship between the CMSR output signal and system parameters, the system parameters are fixed, $a = 0.5$, $r = -0.8$, the interval of b is set to $[0, 10]$, the step size is 0.1, and the change curve of output SNR with b is obtained as shown in Figure 5a where the output SNR is maximum at approximately $b = 6.5$. Then, setting $b = 6.5$, $r = -0.8$, the interval of a is $[0, 2]$, the step size is 0.05, and the change curve of the output SNR with a is obtained, as shown in Figure 5b. The maximum output SNR is obtained at $a = 0.5$ from the figure. Finally, setting $b = 6.5$, $a = 0.5$, the interval of r is $[-5, 5]$, the step size is 0.1, and the change curve of the output SNR with r is obtained, as shown in Figure 5c. Through this figure, it can be inferred that the output SNR reaches its maximum at approximately $r = -0.8$.

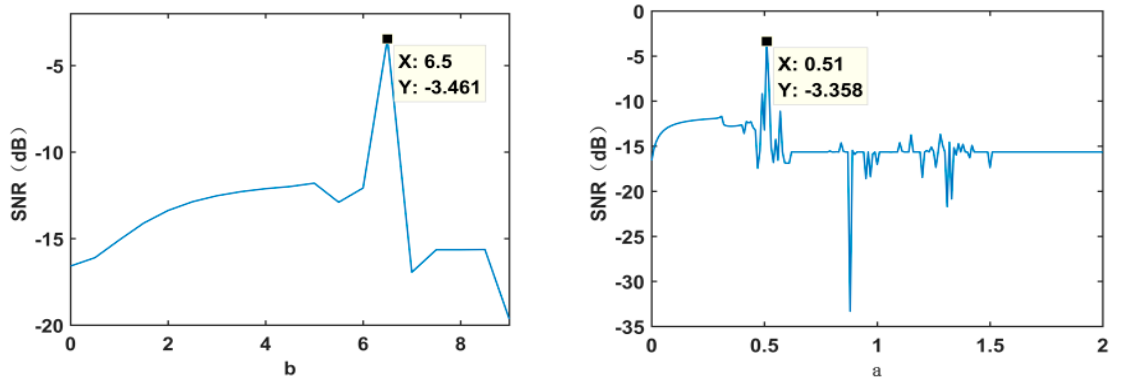


(a) Noiseless signal and amplitude spectrum



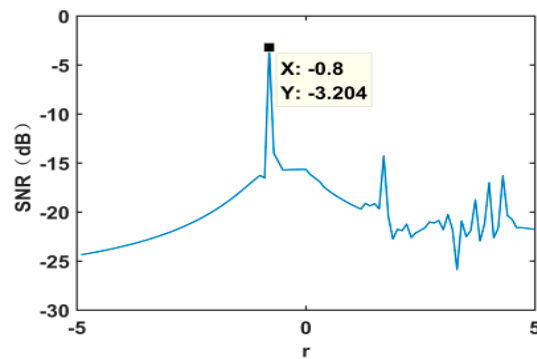
(b) Noise signal and amplitude spectrum

Figure 4. Simulation signal.



(a) Relationship between b and output SNR

(b) Relationship between a and output SNR



(c) Relationship between r and output SNR

Figure 5. Relationship between system parameters and output SNR.

Figure 5 fully expresses that the relationship between the output SNR and system parameters is not linear, but has random uncertainty. The three parameters together determine the output signal of the CMSR system. When $a = 0.5$, $b = 6.5$, $r = -0.8$, the output results of the SR system are as shown in Figure 5. Here, the periodicity of sinusoidal signals and $f_0 = 0.025$ Hz can be clearly identified.

4. Engineering Application

The bearing inner race and rolling element fault data from the Western Reserve University Experimental Center were processed separately to illustrate the effectiveness of the CMSR system [48]. The experimental platform is shown in Figure 6. The 6205-2RS JEM SKF deep groove ball bearing is employed in the experiment. The motor is connected to a dynamometer and torque sensor by a self-aligning coupling. The data were collected from accelerometers on the motor housing at the drive end of the motor. The vibration signals were measured under no-load (0 hp) at a rotating speed of 1797 r/min. Faults were introduced into the test bearings by using an electro-discharge machining method. The fault diameter was 0.007. The vibration signals of the motor bearing were sampled at the frequency of 12,800 Hz and the duration of each vibration signal was 10 s. The original vibration signals were divided into segmentations of samples, and each sample covered 2048 datapoints. According to the theoretical calculation values of fault characteristic frequency, the faults of the outer race, inner race, and rolling element of motor bearing are determined. As a comparison, the experimental signal is denoised by a MSR system.

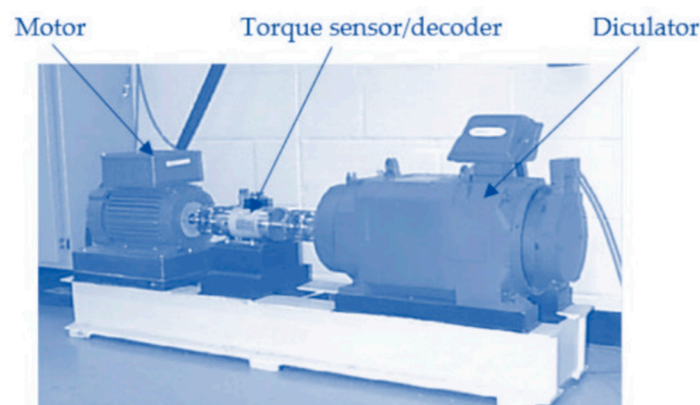


Figure 6. The experimental platform.

Size parameters of bearings are shown in Table 1. The bearing inner race and rolling element fault characteristic frequency is calculated as follows

$$f_{BPF1} = \frac{n}{2} \left(1 + \frac{d}{D} \cos \alpha \right) f_r \quad (14)$$

$$f_{BSF} = \frac{D}{2d} \left[1 - \left(\frac{d}{D} \cos \alpha \right)^2 \right] f_r \quad (15)$$

where f_{BPF1} and f_{BSF} are the fault characteristic frequencies, α is the angular contact angle, d is the roller diameter, D is the bearing pitch diameter, the number of rollers is n , and the frequency shift is f_r .

Table 1. Size parameters of bearings.

Inner Diameter (mm)	Outer Ring Diameter (mm)	Pitch Diameter (mm)	Roller Diameter (mm)	Roller Number	Angular Contact Angle
25.001	51.999	39.04	7.94	9	0

Firstly, the bearing inner race fault is analyzed. The theoretical value of characteristic frequency is 162.2 Hz according to Equation (14) when motor speed is 1797 r/min, sampling length is 8192, and sampling frequency is 12 kHz. For the original vibration signal, Figure 7 is the time-domain waveform and power spectrum. In the power spectrum, there is a significant resonance band at 2000–4000 Hz, and no useful fault characteristic information can be obtained. After bandpass filtering (the filter segment is the resonance band) and envelope processing, the resulting envelope diagram is shown in Figure 8b. Although we can see the fault characteristic frequency from its amplitude spectrum, it cannot be effectively judged by the interference of surrounding noise, and the SNR is -18.85 dB. Figure 8c is the result of using the MSR to process the envelope signal. At this time, the output SNR is improved to -16.3106 dB, system parameters are $a = 84.6$, $b = 0.113$, $R = 1000$, and the high-frequency noise component is restrained, but the noise component of low-frequency is increased to affect the judgment. Figure 7 displays the output result of processing the envelope signal using the CMSR algorithm. The signal in time-domain waveform can be found to be periodic and characteristic frequency f_{BPFI} can be clearly discerned in the amplitude spectrum. The system parameters at this time are $a = -0.19$, $b = 2.28$, $r = -3.13$, $R = 545.96$, and output SNR is -5.27 dB. The feasibility of the CMSR algorithm can be proven by bearing inner race fault data analysis results.

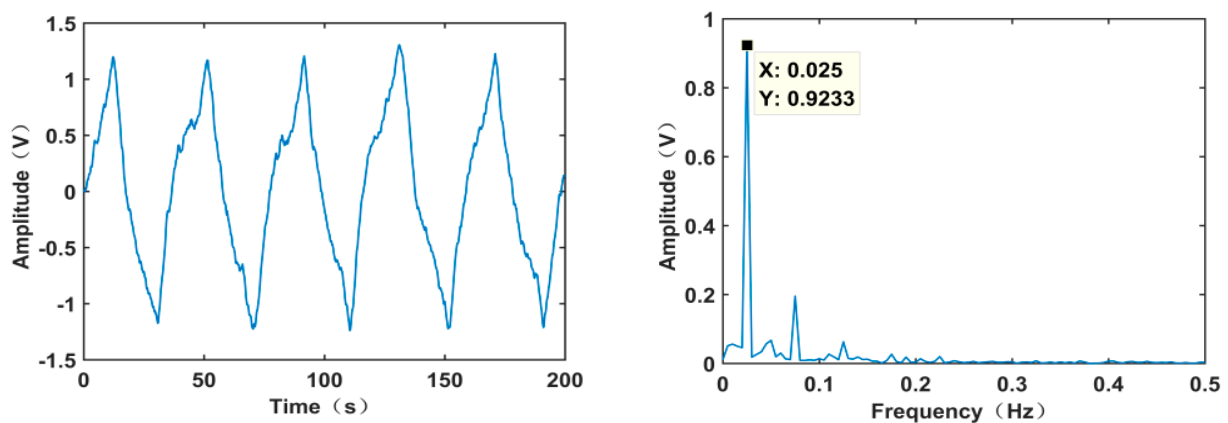
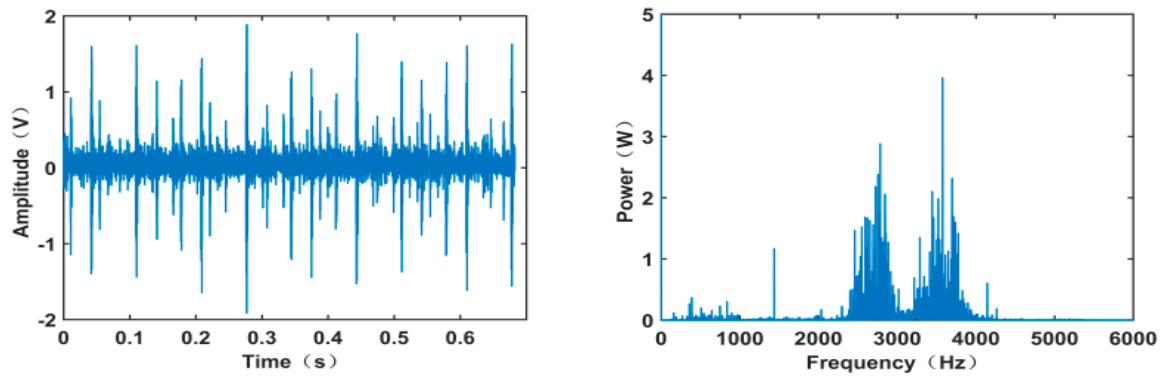
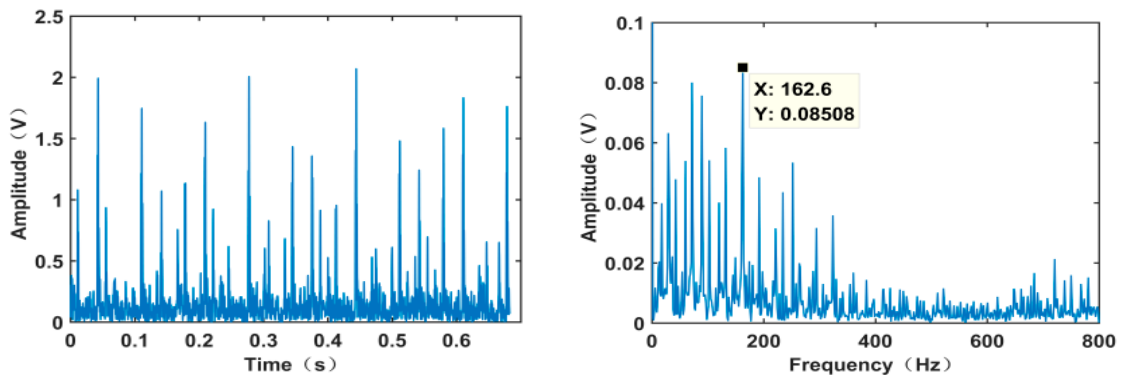


Figure 7. Time-domain waveform and amplitude spectrum of SR output signal.

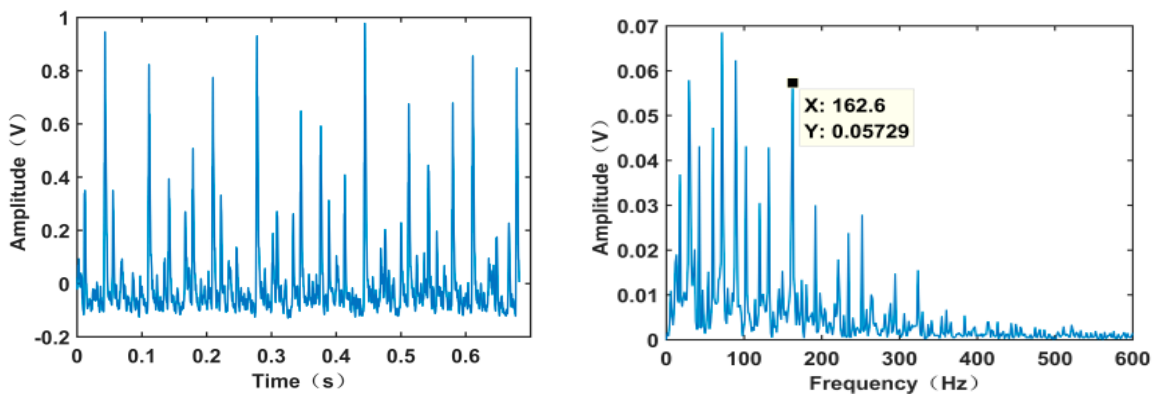
In order to continue to prove the effectiveness of the proposed method for bearing rolling element fault signal, the following experiment must be carried out. First, motor speed is 1797 r/min, sampling length is 4096, and sampling frequency is 12 kHz. The rolling element fault characteristic frequency is, theoretically, $f_{BSF} = 141.17$ Hz. For the original vibration signal, Figure 9a shows its time-domain waveform and power spectrum. Figure 9b is the envelope graph of the bandpass filtering and envelope processing of it, and the calculated SNR of roller failure frequency is -19.67 dB. Then, the MSR algorithm is used to process the envelope signal, $a = 0.12$ and $b = 2.85$ are optimal parameters, the frequency compression scale is $R = 1000$, output SNR is -17.4597 dB. Figure 9c is the output result. Although the high-frequency noise is controlled, the noise component of low-frequency is amplified instead. Finally, the output result of the CMSR system is shown in Figure 9d. The fault characteristic frequency of the rolling element is particularly prominent in the whole spectrum, and other noise frequencies are almost non-existent in the amplitude spectrum. The system parameters at this time are $a = -0.31$, $b = 1.8$, $r = -1.76$, $R = 592.5$. The output SNR = -4.34 dB. The result of the rolling element fault signal analysis again shows the feasibility of the CMSR method.



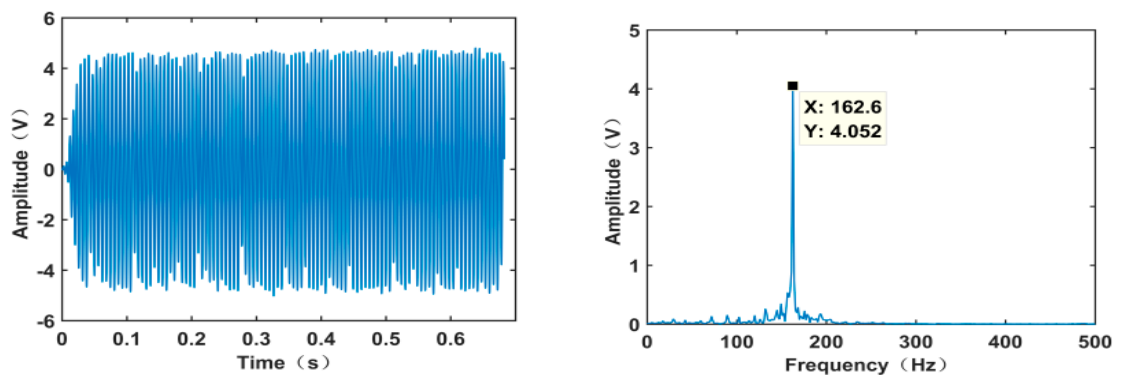
(a) Original vibration signal and power spectrum



(b) Envelope signal and amplitude spectrum

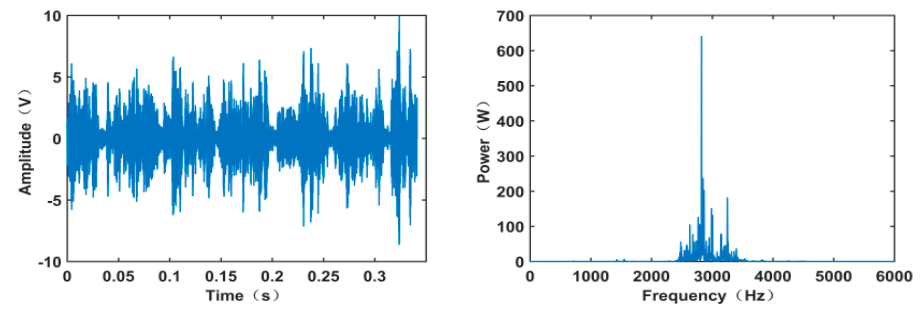


(c) Time-domain waveform and amplitude spectrum of the output signal of a MSR system

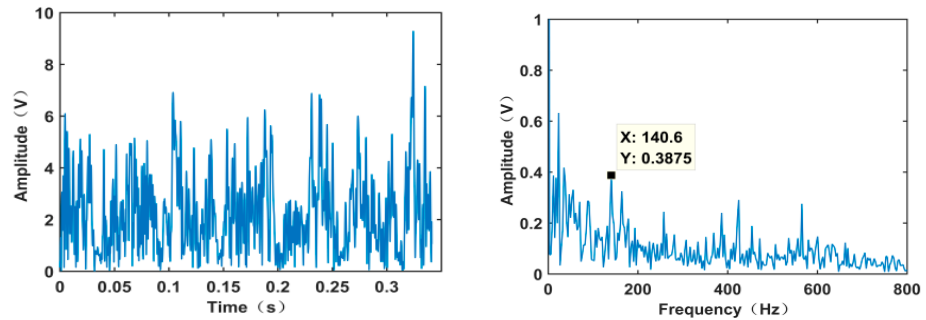


(d) Output signal time-domain waveform and amplitude of the CMSR system

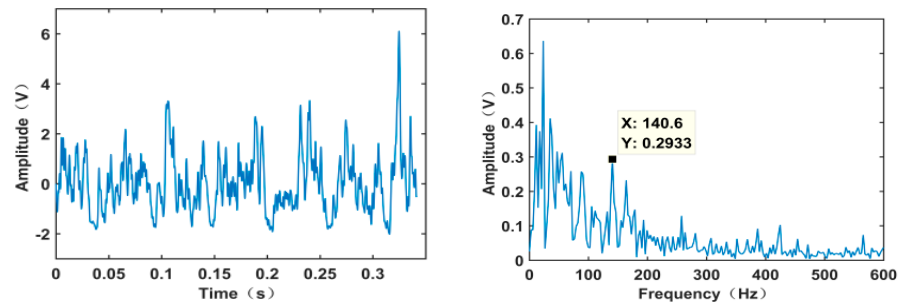
Figure 8. Inner race failure analysis.



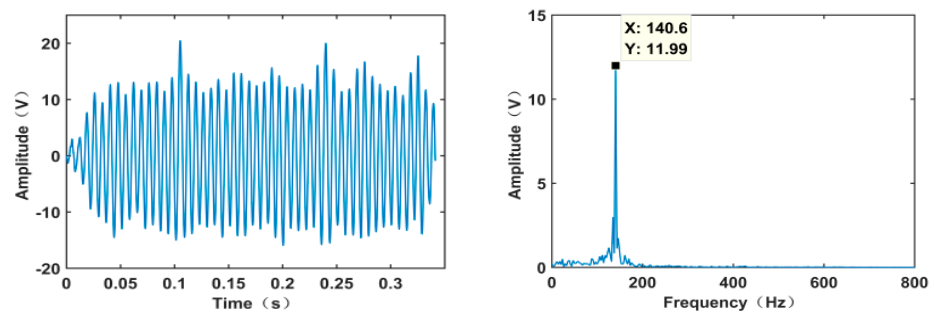
(a) Original vibration signal and power spectrum



(b) Envelope signal and amplitude spectrum



(c) Time-domain waveform and amplitude spectrum of the output signal of MSR system



(d) Output signal time domain waveform and amplitude spectrum of CMSR system

Figure 9. Rolling element signal analysis.

According to the theoretical value and the obtained value for inner race and the rolling element of motor bearings, the calculation error is shown in Table 2.

Table 2. Calculation error between the theoretical value and the obtained value.

Objects	Theoretical Value	Obtained Value	Error
Inner race	162.2 Hz	162.6 Hz	0.4 Hz
Rolling element	141.1 Hz	140.6 Hz	0.5 Hz

It can be seen from Table 2 that the obtained values of the inner race and the rolling element of motor bearings are 162.6 Hz and 140.6 Hz, respectively. Compared with their

theoretical values, the calculation errors between the theoretical values and the obtained values are 0.4 Hz and 0.5 Hz, respectively. The obtained values are infinitely close to the theoretical values, which show that the proposed CMSR system can effectively detect the faults of motor bearings. Therefore, the proposed CMSR system is a weak signal feature extraction method for fault detection in engineering rotating machinery.

5. Conclusions

In this paper, to improve the ability of signal processing for weak bearing signal under the strong noise, a new advancing coupled multi-stable stochastic resonance method with two first-order, multi-stable stochastic resonance systems, namely the CMSR, is proposed to detect motor bearing faults. The CMSR utilizes the output signal-to-noise ratio and seeker optimization algorithm to adaptively optimize and determine the system parameters of the SR. Then, the pre-processed signal is input into the CMSR in order to detect the faults of motor bearings by Fourier transform. In order to prove the effectiveness of the CMSR, the actual vibration data of induction motor bearings are used, and the comparison results with the MSR show that the CMSR system can obtain a higher output SNR to extract weak signal features and realize the fault detection. The advantages of the CMSR system are summarized as follows:

- The CMSR system can detect weak high-frequency signals by combining the variable-scale method;
- With the output SNR as the fitness function of the SOA the parameters of the CMSR system can be determined;
- The engineering data-processing results show that the CMSR system has better filtering performance, higher output SNR, and more effective detection results than traditional SR methods, which has broader prospects for weak signal processing.

Due to the slower computing speed of the CMSR system, we will continue to research the CMSR to improve its computing efficiency in the future. In addition, we will devote ourselves to studying other indicators to complete the detection of unknown characteristic frequency signals. At the same time, the impact of different types of noise on the CMSR system can be further studied and discussed in the future.

Author Contributions: Conceptualization, H.C. (Hongjiang Cui) and Y.G.; methodology, Y.G.; software, H.C. (Hongjiang Cui); validation, W.D. and H.C. (Huayue Chen); data curation, Y.G.; writing—original draft preparation, H.C. (Hongjiang Cui) and Y.G.; writing—review and editing, W.D. and H.C. (Huayue Chen); project administration, H.C. (Huayue Chen); funding acquisition, H.C. (Hongjiang Cui). All authors have read and agreed to the published version of the manuscript.

Funding: This research was funded by the Science Researching Plans of Liaoning Province Education Department under Grant JDL2019003.

Institutional Review Board Statement: Not applicable.

Informed Consent Statement: Not applicable.

Data Availability Statement: <https://csegroups.case.edu/bearingdatacenter/pages/welcome-case-western-reserve-university-bearing-data-center-website> (accessed on 9 June 2021).

Conflicts of Interest: The authors declare no conflict of interest.

References

1. Lu, L.; Yuan, Y.; Wang, H.; Zhao, X.; Zheng, J. A New Second-Order Tristable Stochastic Resonance Method for Fault Diagnosis. *Symmetry* **2019**, *11*, 965. [CrossRef]
2. Sun, J.; Zhang, W.; Lou, S. Adaptive blind extraction of rolling bearing fault signal based on equivariant adaptive separation via independence. *J. Electron. Inf. Technol.* **2020**, *42*, 2471–2477.
3. Jin, T.; Yang, X.; Xia, H.; Ding, H. Reliability index and option pricing formulas of the first hitting time model based on the uncertain fractional-order differential equation with Caputo type. *Fractals* **2020**. [CrossRef]
4. Luo, Z.; Lu, X.; Zhou, Y. EEG feature extraction based on brain function network and sample entropy. *J. Electron. Inf. Technol.* **2021**, *43*, 412–418.

5. AlShorman, O.; Irfan, M.; Saad, N.; Zhen, D.; Haider, N.; Glowacz, A.; AlShorman, A. A review of artificial intelligence methods for condition monitoring and fault diagnosis of rolling element bearings for induction motor. *Shock Vib.* **2020**, *2020*, 8843759. [[CrossRef](#)]
6. Khosravani, M.R.; Nasiri, S.; Weinberg, K. Prediction of fracture in sandwich-structured composite joints using case-based reasoning approach. *Procedia Struct. Integr.* **2018**, *13*, 168–173. [[CrossRef](#)]
7. Jin, T.; Ding, H.; Xia, H.; Bao, J. Reliability index and Asian barrier option pricing formulas of the uncertain fractional first-hitting time model with Caputo type. *Chaos Solitons Fractals* **2021**, *142*, 110409. [[CrossRef](#)]
8. Gui, W.; Lu, Q.; Su, M. A fireworks algorithm-back propagation fault diagnosis algorithm for system-level fault diagnosis. *J. Electron. Inf. Technol.* **2020**, *42*, 1102–1109.
9. Zhao, H.; Li, H.; Jin, Y.; Dang, X.; Deng, W. Feature extraction for data-driven remaining useful life prediction of rolling bearings. *IEEE Trans. Instrum. Meas.* **2021**. [[CrossRef](#)]
10. AlShorman, O.; Alkhatni, F.; Masadeh, M.; Irfan, M.; Glowacz, A.; Althobiani Fkozik, J.; Kozik, J.; Glowacz, W. Sounds and Acoustic emission-based early fault diagnosis of induction motor: A review study. *Adv. Mech. Eng.* **2021**, *13*, 1687814021996915. [[CrossRef](#)]
11. Guo, S.; Zhang, X.; Du, Y.; Zheng, Y.; Cao, Z. Path planning of coastal ships based on optimized DQN reward function. *J. Mar. Sci. Eng.* **2021**, *9*, 210. [[CrossRef](#)]
12. Glowacz, A.; Tadeusiewicz, R.; Legutko, S.; Caesarendra, W.; Irfan, M.; Liu, H.; Brumerick, F.; Gutten, M.; Sulowicz, M.; Daviu, J.A.A.; et al. Fault diagnosis of angle grinders and electric impact drills using acoustic signals. *Appl. Acoust.* **2021**, *179*, 108070. [[CrossRef](#)]
13. Chen, H.; Zhang, Q.; Luo, J.; Xu, Y.; Zhang, X. An enhanced Bacterial Foraging Optimization and its application for training kernel extreme learning machine. *Appl. Soft Comput.* **2020**, *86*, 105884. [[CrossRef](#)]
14. Benzi, R.; Sutera, A.; Vulpiani, A. The mechanism of stochastic resonance. *J. Phys. A Math. Gen.* **1981**, *14*, L453–L457. [[CrossRef](#)]
15. Gammaitoni, L.; Hänggi, P.; Jung, P.; Marchesoni, F. Stochastic resonance. *Rev. Mod. Phys.* **1998**, *70*, 223–287. [[CrossRef](#)]
16. Leng, Y.G.; Leng, Y.S.; Wang, T.Y.; Guo, Y. Numerical analysis and engineering application of large parameter stochastic resonance. *J. Sound Vib.* **2006**, *292*, 788–801. [[CrossRef](#)]
17. Li, T.; Zhou, M. ECG classification using wavelet packet entropy and random forests. *Entropy* **2016**, *18*, 285. [[CrossRef](#)]
18. Tan, J.; Chen, X.; Wang, J.; Chen, H.; Cao, H.; Zi, Y.; He, Z. Study of frequency-shifted and re-scaling stochastic resonance and its application to fault diagnosis. *Mech. Syst. Signal Process.* **2009**, *23*, 811–822. [[CrossRef](#)]
19. Wang, J.; He, Q.; Kong, F. An improved multiscale noise tuning of stochastic resonance for identifying multiple transient faults in rolling element bearings. *J. Sound Vib.* **2014**, *333*, 7401–7421. [[CrossRef](#)]
20. Shi, P.M.; Ding, X.J.; Han, D.Y. Study on multi-frequency weak signal detection method based on stochastic resonance tuning by multi-scale noise. *Measurement* **2014**, *47*, 540–546. [[CrossRef](#)]
21. Zhao, H.; Li, D.; Deng, W.; Yang, X. Research on vibration suppression method of alternating current motor based on fractional order control strategy. *Proc. Inst. Mech. Eng. Part E J. Process. Mech. Eng.* **2017**, *231*, 786–799. [[CrossRef](#)]
22. Zheng, J.; Yuan, Y.; Zou, L.; Deng, W.; Guo, C.; Zhao, H. Study on a Novel Fault Diagnosis Method Based on VMD and BLM. *Symmetry* **2019**, *11*, 747. [[CrossRef](#)]
23. Li, T.; Shi, J.; Zhang, D. Color image encryption based on joint permutation and diffusion. *J. Electron. Imaging* **2021**, *30*, 013008. [[CrossRef](#)]
24. Cai, X.; Zhao, H.; Shang, S.; Zhou, Y.; Deng, W.; Chen, H.; Deng, W.Q. An improved quantum-inspired cooperative co-evolution algorithm with multi-strategy and its application. *Expert Syst. Appl.* **2021**, *171*, 114629. [[CrossRef](#)]
25. Xu, Y.; Chen, H.; Luo, J.; Zhang, Q.; Jiao, S.; Zhang, X. Enhanced Moth-flame optimizer with mutation strategy for global optimization. *Inf. Sci.* **2019**, *492*, 181–203. [[CrossRef](#)]
26. Deng, W.; Xu, J.; Gao, X.; Zhao, H. An enhanced MSIQDE algorithm with novel multiple strategies for global optimization problems. *IEEE Trans. Syst. Man. Cybern. Syst.* **2020**. [[CrossRef](#)]
27. Li, J.; Chen, X.; He, Z. Multi-stable stochastic resonance and its application research on mechanical fault diagnosis. *J. Sound Vib.* **2013**, *332*, 5999–6015. [[CrossRef](#)]
28. Han, D.; An, S.; Shi, P. Multi-frequency weak signal detection based on wavelet transform and parameter compensation band-pass multi-stable stochastic resonance. *Mech. Syst. Signal Process.* **2016**, *70*, 995–1010. [[CrossRef](#)]
29. Lu, S.; He, Q.; Kong, F. Effects of underdamped step-varying second-order stochastic resonance for weak signal detection. *Digit. Signal Process.* **2015**, *36*, 93–103. [[CrossRef](#)]
30. Lei, Y.; Qiao, Z.; Xu, X.; Lin, J.; Niu, S. An underdamped stochastic resonance method with stable-state matching for incipient fault diagnosis of rolling element bearings. *Mech. Syst. Signal Process.* **2017**, *94*, 148–164. [[CrossRef](#)]
31. Zhang, J.; Lin, M. Detection of bearing fault signals based on coupled Bistable system stochastic resonance. *J. China Univ. Metrol.* **2014**, *25*, 51–56. [[CrossRef](#)]
32. Li, J.; Zhang, J.; Li, M.; Zhang, Y. A novel adaptive stochastic resonance method based on coupled bistable systems and its application in rolling bearing fault diagnosis. *Mech. Syst. Signal Process.* **2019**, *114*, 128–145. [[CrossRef](#)]
33. Zhang, G.; Hu, D.; Zhang, T. The analysis of stochastic resonance and bearing fault detection based on linear coupled bistable system under lévy noise. *Chin. J. Phys.* **2018**, *56*, 2718–2730. [[CrossRef](#)]

34. Jin, T.; Ding, H.; Li, B.; Xia, H.; Xue, C. Valuation of interest rate ceiling and floor based on the uncertain fractional differential equation in Caputo sense. *J. Intell. Fuzzy Syst.* **2021**, *40*, 5197–5206. [[CrossRef](#)]
35. Deng, W.; Shang, S.; Cai, X.; Zhao, H.; Zhou, Y.; Chen, H.; Deng, W. Quantum differential evolution with cooperative coevolution framework and hybrid mutation strategy for large scale optimization. *Knowl. Based Syst.* **2021**, *224*, 107080. [[CrossRef](#)]
36. Shao, H.; Chen, J.; Jiang, H.; Yang, Y.; Wu, Z. Enhanced deep gated recurrent unit and complex wavelet packet energy moment entropy for early fault prognosis of bearing. *Knowl. Based Syst.* **2019**. [[CrossRef](#)]
37. Deng, W.; Xu, J.; Zhao, H.; Song, Y. A novel gate resource allocation method using improved PSO-based QEA. *IEEE Tran. Intell. Transp. Syst.* **2020**. [[CrossRef](#)]
38. Jin, T.; Xia, H.; Chen, H. Optimal control problem of the uncertain second-order circuit based on first hitting criteria. *Math. Methods Appl. Sci.* **2021**, *44*, 882–900. [[CrossRef](#)]
39. Hu, B.; Guo, C.; Wu, J.; Tang, J.; Zhang, J.; Wang, Y. An adaptive periodical stochastic resonance method based on the grey wolf optimizer algorithm and its application in rolling bearing fault diagnosis. *J. Vib. Acoust.* **2019**, *141*, 041016. [[CrossRef](#)]
40. Wu, D.; Liao, Y.; Hu, C.; Yu, S.; Tian, Q. An enhanced fuzzy control strategy for low-level thrusters in marine dynamic positioning systems based on chaotic random distribution harmony search. *Int. J. Fuzzy Syst.* **2020**. [[CrossRef](#)]
41. Jin, T.; Yang, X. Monotonicity theorem for the uncertain fractional differential equation and application to uncertain financial market. *Math. Comput. Simul.* **2021**, *190*, 203–221. [[CrossRef](#)]
42. Xu, P.; Jin, Y. Stochastic resonance in multi-stable coupled systems driven by two driving signals. *Phys. A Stat. Mech. Appl.* **2018**, *492*, 1281–1289. [[CrossRef](#)]
43. Zhang, Y.; Yang, G. The optimization of wireless sensor network topology based on FW-PSO algorithm. *J. Electron. Inf. Technol.* **2021**, *43*, 396–403.
44. Dai, C.; Chen, W.; Zhu, Y.; Zhang, X. Seeker optimization algorithm for optimal reactive power dispatch. *IEEE Trans. Power Syst.* **2009**, *24*, 1218–1231.
45. Buchner, A.; Hadrath, S.; Burkard, R.; Kolb, F.; Ruskowski, J.; Ligges, M.; Grabmaier, A. Analytical Evaluation of Signal-to-Noise Ratios for Avalanche- and Single-Photon Avalanche Diodes. *Sensors* **2021**, *21*, 2887. [[CrossRef](#)]
46. Jin, T.; Zhu, Y. First hitting time about solution for an uncertain fractional differential equation and application to an uncertain risk index model. *Chaos Solitons Fractals* **2020**, *137*, 109836. [[CrossRef](#)]
47. Peterson, B.J.; Reichle, R.; Pandya, S.; O'Mullane, M.G.; Mukai, K. Consideration of signal to noise ratio for an imaging bolometer for ITER. *Rev. Sci. Instrum.* **2021**, *92*, 043534. [[CrossRef](#)]
48. Loparo, K.A. Case Western Reserve University Bearing Data Center. Available online: <https://csegroups.case.edu/bearingdatacenter/pages/welcome-case-western-reserve-university-bearing-data-center-website> (accessed on 10 January 2021).